ACS Energy LETTERS

http://pubs.acs.org/journal/aelccp

Rechargeable Metal−Hydrogen Peroxide Battery, A Solution to Improve the Metal−Air Battery Performance

Samira Siahrostami*

Cite This: *ACS Energy Lett.* 2022, 7, 2717−2724

Read Online

ACCESS | Metrics & More | Article Recommendations

ABSTRACT: Rechargeable metal−air batteries are set to play an important role in electrifying the transportation sector and transitioning to a sustainable energy society with zero carbon footprint. However, their performance is vastly hampered by the sluggish kinetics of oxygen redox reactions at the air electrode. Herein, a rechargeable metal−hydrogen peroxide battery is introduced that is air-free and uses onsite generated and reduced hydrogen peroxide (H_2O_2) as an oxygen source for charging and discharging. Replacing oxygen redox reactions with H_2O_2 redox reactions results in a much faster kinetics and a significant improvement in the overall battery performance. Using computationally driven material design with a set of thermodynamic rules, highly stable, active, and selective bifunctional catalyst materials for H_2O_2 generation and reduction are proposed. This technology has the potential to overcome the long-standing issues with metal−air batteries paving the path for advancing the next-generation rechargeable battery technology based on H_2O_2 redox chemistry.

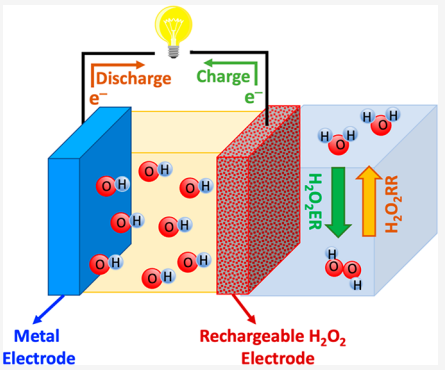

Today there is an increasing interest in improving fuel efficiency in the automotive sector and reducing its dependence on fossil fuels. This has led to a major trend in electrification with a particular focus on clean conversion technologies such as fuel cells, super capacitors, and metal−air batteries. Among them, metal−air batteries are promising next-generation energy storage devices.[1] Their electrochemical cell uses pure metals (such as Zn, Li, and Al) that are oxidized at the anode, an ambient air cathode in which the reduction reaction occurs, and an aqueous or aprotic electrolyte. Metal−Air batteries are of particular interest for use in electric vehicles owing to their high energy density, and high specific capacity. However, their efficiency is vastly hampered by different challenges such as slow kinetics in the air cathode originating from the lack of an oxygen-rich environment and proper catalyst.[1] Their electrolyte dries out once exposed to outside air, and they have limited output with flooding potential. A typical example of them is a zinc−air battery, which has only recently been shown to be rechargeable to 100 times using novel materials.[2] The underlying working mechanism for a zinc-air battery is based on zinc redox reaction at the zinc electrode composed of the zinc anode, an aqueous electrolyte, and an air cathode. Power is produced from water oxidation (oxygen evolution reaction, OER) (eq 1) at the anode and oxygen reduction reaction (ORR) (eq 2) at the cathode.OER:

$$2H_2O \rightarrow O_2 + 4(H^+ + e^-) \quad E^\circ = 1.23V_{RHE} \tag{1}$$

ORR:

$$O_2 + 4(H^+ + e^-) \rightarrow 2H_2O \quad E^\circ = 1.23V_{RHE} \tag{2}$$

where V_{RHE} is voltage versus reversible hydrogen electrode (RHE). Oxygen redox reactions (eq 1 and eq 2) are currently being increasingly used in zinc-air battery research owing to their simplicity. However, the slow kinetics of oxygen redox reactions has long been known as the largest factor limiting the current and power density and overall conversion efficiency of the zinc-air battery. The fundamental understanding of the OER and ORR has been largely based on the surface science approach,[3−5] which has enabled direct theoretical investigations of reaction mechanisms on model systems. Both reactions are accompanied by four coupled proton electron transfers involving three different oxygen intermediates, namely, OOH*, O*, and OH*. High cathodic and anodic overpotential losses have been reported for both ORR and OER even using state-of-the-art catalysts for those reactions.

Received: June 21, 2022
Accepted: July 20, 2022

https://doi.org/10.1021/acsenergylett.2c01417
ACS Energy Lett. 2022, 7, 2717−2724

One of the most important achievements of the surface science approach and density functional theory (DFT) calculations has been in explaining the large OER and ORR overpotentials for the studied classes of materials.[4,5] On the basis of this analysis it has been demonstrated that the correlations between binding energies of different oxygen intermediates are obeyed on any catalyst surface.[6−10] Because of these correlations it is impossible to tune the binding energy of one intermediate without affecting the binding energy of the other on any catalyst material. This results in fixing the energy difference between OH* and OOH* intermediates at ~3.2 ± 0.2 eV.[7−9] The fact that all the so-far known and examined materials follow similar correlations between binding energies of different oxygen intermediates poses a large negative impact on their activity toward ORR and OER. Because it takes two proton-coupled electron transfer steps to go from OOH* to OH*, a potential of at least 3.2 eV/2e = 1.6 V is needed to complete these reaction steps. However, the thermodynamics limit is 1.23 V, which means that even the best catalyst surfaces will have an overpotential of ~1.6 − 1.2 V = 0.4 V for either the ORR or OER.[7−9] This in turn makes it impossible to achieve the maximum efficiency in metal-air batteries for oxygen redox reactions. A variety of approaches has been proposed to overcome this limitation, among which porous materials such as metal−organic frameworks,[11] molecular catalysts with a diporphyrin structure,[12] and catalysts with confinement[13,14] have been heavily investigated. An alternative approach to overcome the limitations with oxygen redox reactions is to switch to a different oxygen source such as hydrogen peroxide.

In comparison to O_2, hydrogen peroxide (H_2O_2), a benign oxidizing agent, provides an oxygen-rich environment to react with the electrode surfaces with a much faster kinetics than oxygen.[8] Unlike oxygen redox reactions that involve four coupled proton−electron transfers, H_2O_2 redox reactions are accompanied by two coupled proton−electron transfers (eq 3 & 4) with one intermediate and a much lower activation barrier. Moreover, H_2O_2 is liquid, which makes it an ideal energy carrier alternative to hydrogen.[15] Given that storage and transportation of H_2O_2 is relatively simple compared with H_2, development and widespread application of technologies such as H_2O_2-based fuel cells are of particular interest. The H_2O_2-based fuel cells have been long known and investigated to generate electricity.[16] Their particular application is in deficient environments such as space and ocean and space explorations.[17] This technology adapts the H_2O_2 reduction reaction (H_2O_2RR, eq 3) at the cathode instead of the ORR (eq 2). eq 3b shows the mechanism of hydrogen peroxide reduction reaction involving OH* as the sole intermediate.

$$H_2O_2RR: \quad H_2O_2 + 2(H^+ + e^-) \rightarrow 2H_2O \qquad E^\circ = 1.76V_{RHE} \tag{3}$$

$$H_2O_2 + (H^+ + e^-) \rightarrow OH^* + H_2O \tag{3a}$$

$$OH^* + (H^+ + e^-) \rightarrow H_2O \tag{3b}$$

$$H_2O_2ER: \quad 2H_2O \rightarrow H_2O_2 + 2(H^+ + e^-) \qquad E^\circ = 1.76V_{RHE} \tag{4}$$

$$H_2O \rightarrow OH^* + (H^+ + e^-) \tag{4a}$$

$$OH^* + H_2O \rightarrow H_2O_2 + (H^+ + e^-) \tag{4b}$$

Hydrogen peroxide has also been used as an oxygen source in batteries. In 1994, a dual-channel aluminum hydrogen peroxide battery was introduced by Licht et al. that used oxidation of aluminum in the anode and reduction of hydrogen peroxide in the aqueous solution for an overall battery discharge (eq 5).[18] Ir/Pd modified porous nickel cathode was used to separate the catholyte and anolyte chambers. A power density of 1 W/cm^2 was reported for this battery with an open-circuit voltage of 1.9 cm^2 mA^{-1}.

$$2Al + 3H_2O_2 + 2OH^- \rightarrow 2AlO_2^- + 4H_2O \qquad E = 2.3\ V \tag{5}$$

Similarly, H_2O_2 has been recently used in a zinc−H_2O_2 battery by Xu et al.[19] A superior high rate discharging performance, 23% higher than a normal Zn-air battery, was reported. The authors also set up a two-serial Zn−H_2O_2 battery to light a red light-emitting diode (LED) array.[19] Both reports by Licht et al. and Xu et al. certify successful minimization of the battery dependence on oxygen via discharge but make use of manually added H_2O_2 in the cathode.

In recent years, significant advances have been made in developing electrochemical processes for onsite and local production of H_2O_2.[20,21] Water electrolysis (H_2O_2ER, eq 4) has attracted particular attention owing to its simplicity and potential for production of hydrogen peroxide in remote locations.[22−31] The H_2O_2ER is the reverse reaction of the H_2O_2RR and similarly involves OH* as the only intermediate (eqs 4a & 4b).

Herein we propose a new rechargeable metal−H_2O_2 battery, which completely relies on onsite generated and consumed H_2O_2 for charging and discharging cycles, respectively. The conceptual idea will be thoroughly explained in the next section. In brief, however, the idea is to design a completely air-free battery in which water is oxidized to H_2O_2 (H_2O_2ER, eq 4) at the anode during the charging process and H_2O_2 is reduced back to water (H_2O_2RR, eq 3) at the cathode during the discharge. To realize this, efficient H_2O_2ER and H_2O_2RR catalysis is critical for the efficiency of the whole rechargeable metal−H_2O_2 battery. We use computational material design and thermodynamic analysis to guide us as we look for catalyst materials that meet the requirements for such a design. The proposed design represents an innovative idea well worth pursuing.

Rechargeable Metal−H_2O_2 Battery—Conceptual Idea. As discussed in the Introduction, the large overpotential associated with the oxygen redox reactions in metal-air batteries originates from their nature of four coupled proton−electron transfers that involve three oxygen intermediates whose interactions with a catalyst surface must be mutually optimized. For reactions with one intermediate such as hydrogen evolution reaction (HER) or hydrogen oxidation reaction (HOR), this problem does not occur.[32] Thus, the activity can be optimized through identifying a catalyst with optimal binding properties for that sole intermediate. Hence if the oxygen can be replaced by another oxygen rich agent (fuel) with redox reactions involving one intermediate, the overall cell performance in a rechargeable battery can be maximized. Hydrogen peroxide makes an ideal and viable alternative fuel with promise for application under air-deficient conditions. It has high oxygen storage capacity (~1600 times more than air), much faster kinetics than oxygen, and convenient production and consumption. In the novel rechargeable metal-H_2O_2 battery introduced herein, onsite H_2O_2ER (at the anode) and H_2O_2RR (at the cathode) take place during the charging and discharging process, respectively

https://doi.org/10.1021/acsenergylett.2c01417
ACS Energy Lett. 2022, 7, 2717−2724

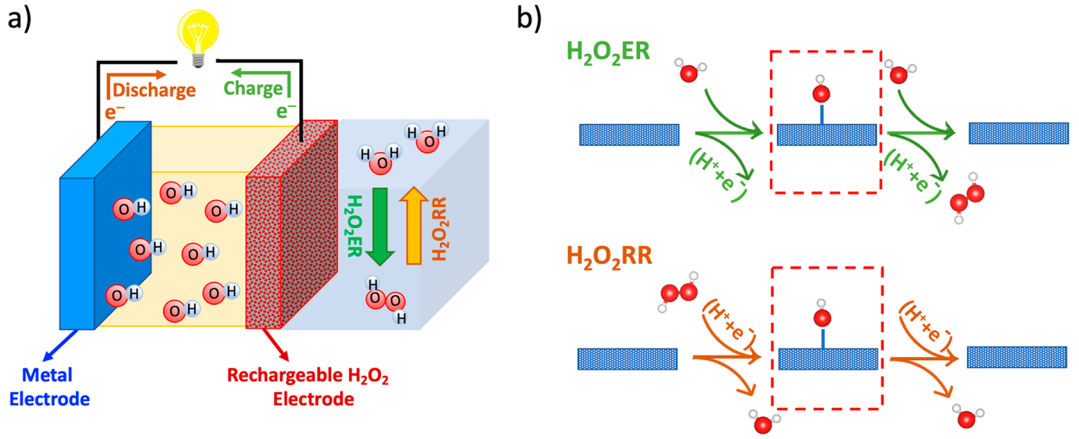

Figure 1. (a) Schematic representation of the rechargeable metal-H_2O_2 battery. (b) Schematics of the mechanism for H_2O_2ER and H_2O_2ER. Red dashed line indicates OH* as the common intermediate for both reactions.

(Figure 1a). Both H_2O_2RR and H_2O_2ER involve one oxygen intermediate, that is, OH* (Figure 1b). Thus, this design, in principle, overcomes the limitations of oxygen redox reactions in zinc-air batteries. Moreover, the input and output of charging and discharging of the battery is water.

Since the standard redox potential for H_2O_2RR and H_2O_2ER is 1.76 V, it represents a highly oxidizing condition, and only some oxide/perovskites would be conceivable to show long-term stability under such reaction conditions. Other challenges are related to the activity and selectivity of the catalyst materials used for anode and cathode reactions. A low-cost, stable bifunctional catalyst that can selectivity generate and reduce H_2O_2 with high efficiency would make an ideal rechargeable battery with a much faster kinetics than current metal-air batteries. In the following we will discuss the challenges and advances in catalyst discovery for both H_2O_2ER and H_2O_2RR.

Materials for H_2O_2ER (Anode Reaction, Charging Process). Over the past few years, there have been a lot of improvements in discovering new catalyst materials for selective and active H_2O_2ER.[22−31] Computational guidance based on thermodynamics has been critical both in defining the selectivity and activity descriptors as well as identifying catalyst materials with superior properties.[20,31,33]

A large library of perovskites (∼560) with cubic structure and ABO_3 composition examined by Montoya et al.[34] has been used to mark the most active catalysts for H_2O_2ER as reported in ref 20. However, as pointed out in ref 20, not all these perovskites are stable under the high oxidation potential of H_2O_2ER. The Materials Project database[35] can be used to successfully narrow down the most stable perovskites as summarized in Figure 2a. There are almost 2000 perovskite structures in the Materials Project database. Thermodynamic stability is the first important metric, which we set to the E above Hull equal to zero to only include ABO_3 structures that are stable with respect to decomposition at the same, fixed chemical composition. Structures with a decomposition energy of zero exhibit the highest stability in the Materials Project database. This narrows down the search to 800 ABO_3 perovskites. Electrochemical stability is the second metric, which considers the most stable perovskites under electrochemical conditions (i.e., pH = 8 and 11 with applied electrode potentials of 2.23 and 2.41 V vs standard hydrogen electrode (SHE), respectively). For this step a Pourbaix diagram analyzer, introduced by Persson, et al.,[36] Python Material Genome (Pymatgen[37]), and Materials Project[35] can be used cooperatively. The electrochemical stability threshold is set to 0.2 eV for the decomposition energy,[36,38] which is defined as the difference between the Gibbs free energies of perovskites and the most stable product they are decomposed to in aqueous media.[36,39] Using this stability analysis, a list of 34 stable candidates can be identified (Figure 2b) that are potentially interesting for H_2O_2ER. We note that the stability analysis based on the Pourbaix diagram analyzer is established on the basis of sole thermodynamic analysis with no consideration of the possible kinetic stability as a result of a slow dissolution process.[36] However, on the one hand, previous studies show that materials such as $BiVO_4$ that do not come out as a stable material from the Pourbaix diagram analysis can survive the anodic H_2O_2ER conditions for several hours.[40] On the other hand, different approaches can be taken to increase the stability of those materials. For example, doping $BiVO_4$ with gadolinium has been used as a strategy to improve the long-term stability of $BiVO_4$ by preventing the leaching of vanadate ions.[28] In this study the Pourbiax diagram analysis has been used to mark the materials that inherently have high stability, not taking into account the ones that may not be thermodynamically stable but may show kinetic stability as a result of a slow dissolution process under reaction conditions.

Among the above 34 stable materials, some (marked by a red oval) have already been studied computationally for oxygen evolution reaction and reported in the previous literature.[26,27] Figure 2c shows the calculated limiting potentials for these perovskites as well as the other suggested oxide/perovskites in the literature[26−28,33,41] for H_2O_2ER. A blue rectangle marks the oxides/perovskites that have been experimentally verified in the literature as selective and active catalysts for H_2O_2ER. Some of them have proven to have long-term durability such as ZnO[26] and $CaSnO_3$.[27,33] It remains interesting to experimentally investigate the electrochemical properties (activity and selectivity) of the newly identified perovskites in this study, that are, $LaNiO_3$, $LaCuO_3$, $LaGaO_3$, $LaZnO_3$, $SrNiO_3$, and $SrTiO_3$, for H_2O_2ER. These perovskites have been synthesized and used in the literature for different applications including but not limited to catalysis. For example, $CaTiO_3$[42] and $SrTiO_3$[43] have been recently studied as photocatalysts for water splitting. La-based perovskites have long been considered as potential cathode materials for solid oxide fuel cells.[44] In terms of synthetic feasibility, both solid-state reaction and wet chemical routes have been used and reported in the literature for

https://doi.org/10.1021/acsenergylett.2c01417
ACS Energy Lett. 2022, 7, 2717−2724

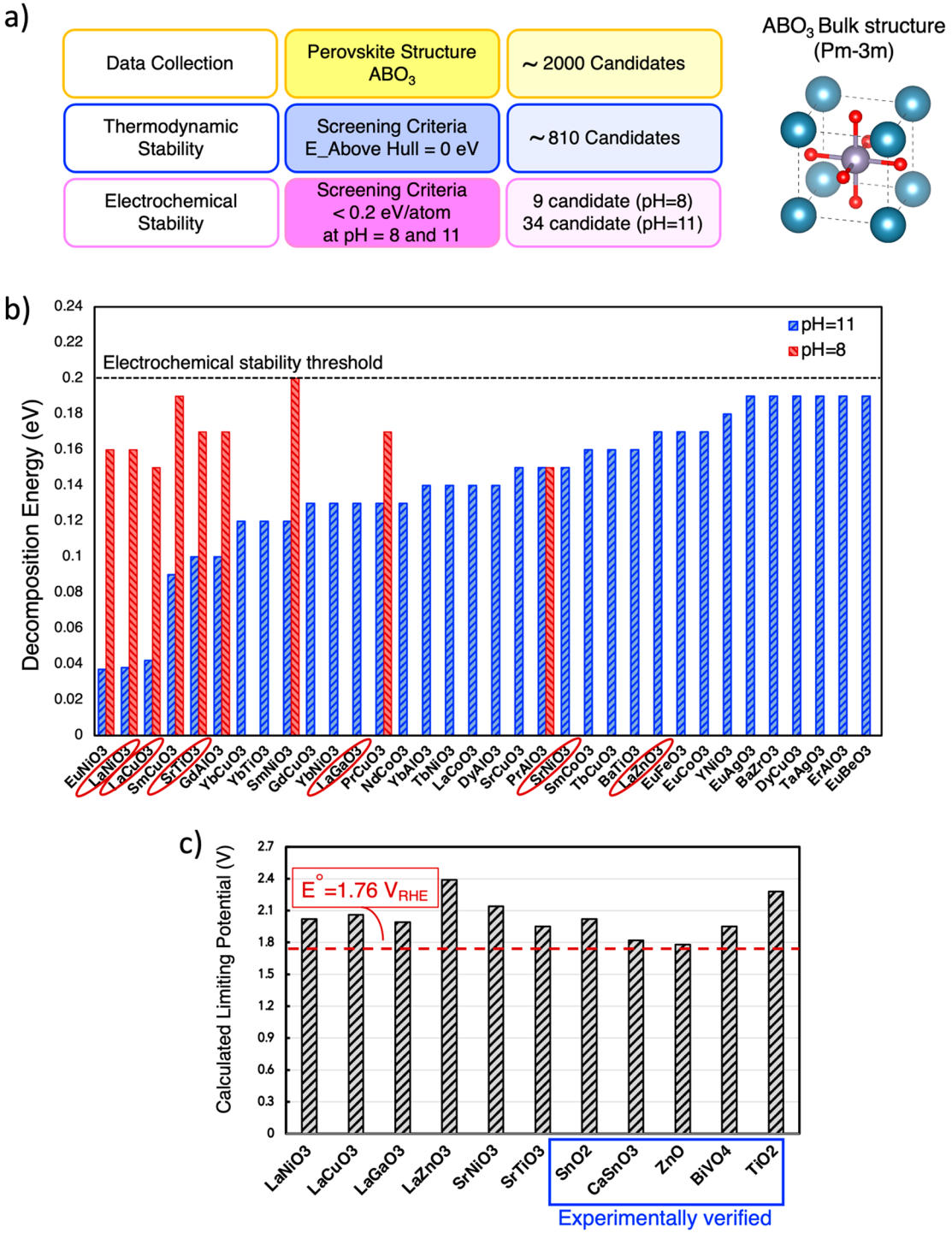

Figure 2. (a) Summary of the approach taken to screen the most stable perovskite materials. (b) Shortlisted perovskites with decomposition energies less than 0.2 eV as electrochemical stability threshold (black dashed line). (c) Reported calculated limiting potential for the perovskites marked by red ovals in (b) as well as oxides taken from refs 5 & 20.

preparing perovskites.[44] The downside of the solid-state route is the lack of formation of a pure single phase due to slow reaction kinetics and a lack of control of particle size and surface area. Different wet chemical routes such as combustion, coprecipitation, and citrate-gel methods have been used to address the challenges with the solid-state method. The advantage of these methods is that they provide mixing of the elements at an atomic scale, which accelerates pure phase formation. Moreover, these methods use lower calcination temperatures, which provides more control over the particle size, morphology, and surface area.

Materials for H_2O_2RR (Cathode Reaction). The evolution of the research in the field of direct H_2O_2 fuel cell (DHPFC) provides a good hint for identifying suitable catalysts for H_2O_2RR.[16] DHPFC, first designed by Hasegawa et al. in 2004,[45] uses oxidation and reduction of H_2O_2 to generate electricity. In this cell H_2O_2RR (eq 3) occurs in the acidic electrolyte, and

https://doi.org/10.1021/acsenergylett.2c01417
ACS Energy Lett. 2022, 7, 2717−2724

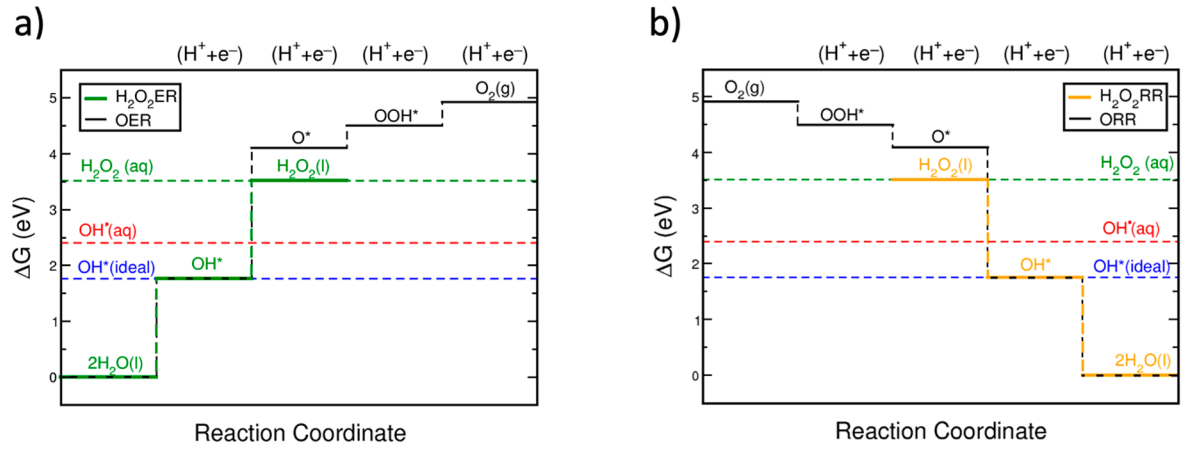

Figure 3. (a) Free energy diagram of a desired catalyst material with high selectivity and activity for H_2O_2ER (green). (b) Free energy diagram of a desired catalyst material with high selectivity and activity for H_2O_2RR (orange). Black shows the competing OER and ORR reaction pathways in each case.

H_2O_2 oxidation reaction (H_2O_2OR, eq 6) happens in the alkaline electrolyte.[45]

$$H_2O_2 + 2OH^- \rightarrow O_2 + H_2O + 2e^- \quad E^\circ = 0.0649\ \text{V} \tag{6}$$

Earlier versions of catalysts tested for H_2O_2RR were based on the noble metals such as Pt, Pd,[46] and their alloys.[47] Most recently, oxides and perovskites have been heavily investigated under an alkaline condition to overcome challenges associated with the stability of the catalysts under H_2O_2RR conditions. Cobalt-based catalysts, particularly spinel structures such as Co_3O_4[48] and $[(Cu_{0.30}Co_{0.70})Co_2O_4]$,[49] show excellent H_2O_2RR properties. Perovskites such as A_2BO_4-type and $La_{1-x}Sr_xMnO_3$ have proven to be promising alternative catalyst materials for H_2O_2RR.[50−52] One common challenge in H_2O_2RR is simultaneous reduction and oxidation of H_2O_2 at the surface of the electrocatalyst. The net reaction is unproductive disproportionation and decomposition of H_2O_2 to oxygen and water, generating a mixed potential on the electrode. This phenomenon is problematic because it diminishes the maximum power of the cell and wastes the H_2O_2 fuel lowering the overall fuel efficiency. Therefore, an ideal catalyst for H_2O_2RR must be stable under reaction conditions and present a strong selectivity toward reduction of H_2O_2 rather than its decomposition. The successful design of efficient catalyst materials for H_2O_2RR would be achieved with computational guidance.

Unlike H_2O_2ER, less attention has been paid to systematically studying the catalysts materials for H_2O_2RR using computational guidance. The only study in the literature is the computational work by Siahrostami et al. in 2013, in which they provided a lead for identifying selective and active catalyst materials for H_2O_2RR.[8] Using DFT calculations they investigated the oxidation and disproportionation pathways of H_2O_2 and identified thermodynamic criteria and descriptors. On the basis of this study, the most active and selective catalyst for H_2O_2RR should have $\Delta G_{OH^*} = 1.76$ eV and $\Delta G_{OH^*} > 3.52$ eV, respectively. This thermodynamic hint led to finding $SrTiO_3$ as the most active and selective catalyst material for this reaction.[8]

Bifunctional Materials for H_2O_2ER and H_2O_2RR. Comparing H_2O_2RR and H_2O_2ER discussed above, we find that both reactions share similar selectivity and activity descriptors because they both share OH* as the critical intermediate (as marked by a red rectangle in Figure 1b). Thus, in principle, the catalyst materials that were discovered as the most efficient for H_2O_2ER will be also effective for H_2O_2RR. This scenario is an analogy to HER and HOR, where H* is the descriptor for both reactions, and the most active catalyst for HER (e.g., Pt) is also the most active one for HOR.[9] Using this guidance, we can identify bifunctional materials that work for both H_2O_2RR and H_2O_2ER. Since the computational and experimental materials discovery is more mature in the H_2O_2ER, we base our search for identifying bifunctional materials on the findings in this area. The analysis in Figure 2 shows several new perovskites ($LaGaO_3$, $LaNiO_3$, $LaCuO_3$, $LaZnO_3$, $SrNiO_3$, and $SrTiO_3$) that are potentially promising for H_2O_2RR in addition to previously reported stable and active oxide/perovskite materials (ZnO, $CaSnO_3$).

In the following we use the computational hydrogen electrode (CHE) model, which exploits that the chemical potential of a proton−electron pair is equal to gas-phase H_2 at standard conditions to identify trends in activity for both H_2O_2RR and H_2O_2ER across the above-mentioned oxides/perovskites. The electrode potential is taken into account by shifting the electron energy by $-eU$, where e and U are the elementary charge and the electrode potential, respectively.[3] The calculated limiting potentials (U_L) for the H_2O_2RR and H_2O_2ER to occur are defined as the lowest and highest potentials, at which all the reaction steps in the free energy diagram (Figure 3) are downhill, respectively, following ref 31.

Figure 3a,b show the free energy diagrams for H_2O_2RR and H_2O_2ER, respectively, at U = 0.0 V, along with their corresponding competing reaction pathways (i.e., ORR and OER, respectively). The free energy of H_2O_2 and OH radical are marked by green and red dashed lines, respectively. The blue dashed lines represent the optimum free energy of the OH* intermediate (1.76 eV) on an ideal catalyst for which zero overpotential is required to drive both H_2O_2RR and H_2O_2ER. Selectivity toward both H_2O_2RR and H_2O_2ER is critical for a bifunctional catalyst. As discussed above, both reactions are sensitive to formation of O*. For the H_2O_2ER, further oxidation of adsorbed OH* to O* will largely limit the selectivity toward H_2O_2. Similarly, in the H_2O_2RR oxidation of H_2O_2 to O* instead of its reduction to OH* will result in disproportionation and decomposition with no energy gain.[8] Therefore, in order to decrease the selectivity toward the pathways that result in forming O* and direct the selectivity toward two-electron routes

https://doi.org/10.1021/acsenergylett.2c01417
ACS Energy Lett. 2022, 7, 2717−2724

in H_2O_2RR and H_2O_2ER, catalysts that adsorb O* weakly are desired. At the same time, O* adsorption energy should be sufficiently strong to dissociate the water molecule and provide a good thermodynamic driving force, for the two-electron pathways. The free energy of H_2O_2 formation is twice the equilibrium potential for eq 4, that is, 3.52 eV. Therefore, the catalyst should have $\Delta G_{O*} \gtrsim 3.52$eV. In addition, because the *O and *OH energies are generally found to linearly scale with each other ($\Delta G_{O*} = 2\Delta G_{OH*} + 0.28$),[53] this sets a lower limit for OH* free energy at $\Delta G_{OH*} \gtrsim \frac{3.5}{2} - \frac{0.28}{2} \approx 1.6$ eV for both H_2O_2RR and H_2O_2ER. The upper limit for ΔG_{OH*} is set by the free energy of OH radical formation in the solution, since too weak OH* free energy with $\Delta G_{OH*} > \sim 2.4$ eV drives both H_2O_2RR and H_2O_2ER reactions toward OH radical formation. Hence, the combined thermodynamic criteria and scaling relation indicates a selective catalyst for H_2O_2RR and H_2O_2ER should have $\sim 1.6 < \Delta G_{OH*}$, eV < 2.4. This selectivity region is highlighted in Figure 4 for the H_2O_2RR (orange) and H_2O_2ER (green). Thus, the thermodynamic analysis suggests that ZnO, $CaSnO_3$, $LaGaO_3$, $LaCuO_3$, $LaZnO_3$, and $SrNiO_3$ are selective bifunctional catalysts to both generate and reduce H_2O_2.

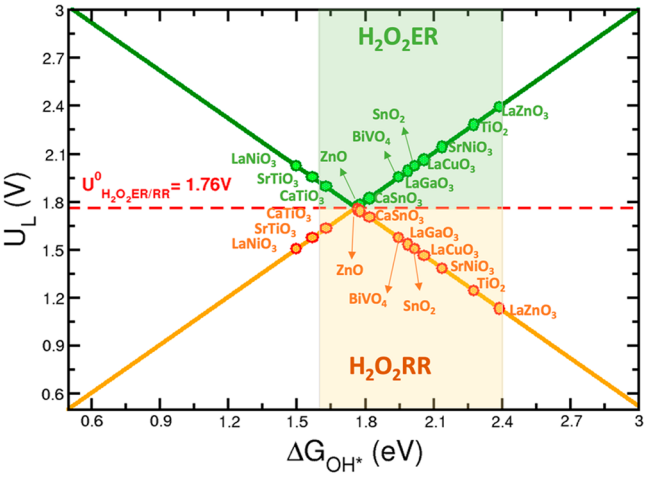

Figure 4. Activity volcano plot for H_2O_2RR (orange) and H_2O_2ER (green). Red dashed line indicates the standard redox potential of 1.76 × V_{RHE} for both H_2O_2RR and H_2O_2ER.

Apart from selectivity, activity is another critical factor in determining suitable bifunctional catalyst materials for H_2O_2RR and H_2O_2ER. Figure 3b shows the activity volcano plots based on the Sabatier principle, which relates the calculated limiting potentials to the adsorption free energy of the descriptor, that is, OH* (ΔG_{OH*}) for both H_2O_2RR (orange) and H_2O_2ER (green). As noted above, the equilibrium potential for both reactions is 1.76 V as marked by the red dashed line. To establish the volcano relationship, we follow the mechanisms mentioned in (3a,b) for H_2O_2RR and 4a,b for H_2O_2ER. For the H_2O_2RR, the first elementary step (3a) involves reduction of H_2O_2 to form OH* (ΔG_{3a}, eq 7). Second proton−electron transfer (3b) reduces OH* to H_2O (ΔG_{3b}, eq 8). Thus, the limiting potential for H_2O_2RR is determined by either formation of OH* from H_2O_2 (ΔG_{3a}) or reduction of OH* to H_2O (ΔG_{3b}).

$$\Delta G_{3a} = \Delta G_{OH*} + \Delta G_{H_2O} - \Delta G_{H_2O_2} \quad (7)$$

$$\Delta G_{3b} = \Delta G_{H_2O} - \Delta G_{OH*} \quad (8)$$

$$U_{L,3a} = \frac{\Delta G_{3a}}{-e} = -\Delta G_{OH*} + 3.52 \quad (9)$$

$$U_{L,3b} = \frac{\Delta G_{3b}}{-e} = \Delta G_{OH*} \quad (10)$$

where $U_{L,3a}$ and $U_{L,3b}$ are the corresponding calculated limiting potentials for the 3a and 3b elementary reactions, respectively.

Similarly, for the H_2O_2ER the first elementary step (4a) involves deprotonation (oxidation) of H_2O to form OH* (ΔG_{4a}, eq 11). The second elementary step (4b) is deprotonation (oxidation) of OH* and combination with H_2O to form H_2O_2 (ΔG_{4b}, eq 12). Thus, the limiting potential for H_2O_2ER is determined by either formation of OH* from H_2O (ΔG_{4a}) or oxidation of OH* + H_2O to form H_2O_2 (ΔG_{4b}).

$$\Delta G_{4a} = \Delta G_{OH*} - \Delta G_{H_2O} \quad (11)$$

$$\Delta G_{4b} = \Delta G_{H_2O_2} - \Delta G_{OH*} - \Delta G_{H_2O} \quad (12)$$

$$U_{L,4a} = \frac{\Delta G_{4a}}{-e} = -\Delta G_{OH*} \quad (13)$$

$$U_{L,4b} = \frac{\Delta G_{4b}}{-e} = \Delta G_{OH*} - 3.52 \quad (14)$$

where $U_{L,4a}$ and $U_{L,4b}$ are the corresponding calculated limiting potentials for the 4a and 4b elementary reactions, respectively.

The theoretical overpotential is defined as the difference between the calculated limiting potential and equilibrium potential (1.76 V for the two-electron path). Since the overpotential is governed by the binding of OH* to the catalyst surface, controlling the overpotential is a matter of tuning the free energy of OH*.[3] An OH* free energy (ΔG_{OH*}) of 1.76 eV, when calculated at zero potential and relative to liquid water, will result in zero overpotential. The calculated theoretical limiting potential for $LaGaO_3$ is 1.99 V, and hence it has a theoretical overpotential of ~0.23 V for both H_2O_2RR and H_2O_2ER. Thus, $LaGaO_3$ together with previously reported ZnO and $CaSnO_3$ make the most promising bifunctional catalyst materials for the proposed rechargeable metal−hydrogen peroxide battery in this study.

Metal−Air batteries are one of the most promising next-generation energy technologies and are deemed to play an important role in electrifying the transportation sector and reducing the carbon footprint. However, the challenges associated with the air electrode such as slow kinetic of oxygen redox reactions hinders their widespread application. In this study, I proposed a novel rechargeable metal−hydrogen peroxide battery that has the potential to overcome the challenges associated with metal-air batteries. This battery relies on onsite generated and reduced hydrogen peroxide (hydrogen peroxide redox reactions, H_2O_2ER and H_2O_2RR) for charge and discharge rather than oxygen redox reactions. The hydrogen peroxide redox reactions have much faster kinetics, which significantly benefit the overall performance of the rechargeable metal−hydrogen peroxide battery. Moreover, the onsite production and reduction of hydrogen peroxide makes the battery entirely self-governing with no need for external injection of hydrogen peroxide. This also avoids the long-term stability issue associated with loaded hydrogen peroxide. By combining the computational and thermodynamic guidance I provided guidelines for identifying stable, selective, and active

https://doi.org/10.1021/acsenergylett.2c01417
ACS Energy Lett. 2022, 7, 2717−2724

bifunctional catalyst materials to drive hydrogen peroxide redox reactions successfully and efficiently.

AUTHOR INFORMATION

Corresponding Author

Samira Siahrostami − *Department of Chemistry, University of Calgary, Calgary T2N 1N4 Alberta, Canada;* orcid.org/0000-0002-1192-4634; Email: samira.siahrostami@ucalgary.ca

Complete contact information is available at: https://pubs.acs.org/10.1021/acsenergylett.2c01417

Notes

The author declares no competing financial interest.

ACKNOWLEDGMENTS

The author acknowledges the support from the University of Calgary's Canada First Research Excellence Fund Program, the Global Research Initiative in Sustainable Low Carbon Unconventional Resources.

REFERENCES

(1) Li, Y.; Lu, J. Metal-Air Batteries: Will They Be the Future Electrochemical Energy Storage Device of Choice? *ACS Energy Lett.* **2017**, *2* (6), 1370−1377.

(2) Zhang, X.; Wang, X.-G.; Xie, Z.; Zhou, Z. Recent Progress in Rechargeable Alkali Metal−Air Batteries. *Green Energy Environ* **2016**, *1* (1), 4−17.

(3) Nørskov, J. K.; Rossmeisl, J.; Logadottir, A.; Lindqvist, L.; Kitchin, J. R.; Bligaard, T.; Jónsson, H. Origin of the Overpotential for Oxygen Reduction at a Fuel-Cell Cathode. *J. Phys. Chem. B* **2004**, *108* (46), 17886−17892.

(4) Kulkarni, A.; Siahrostami, S.; Patel, A.; Nørskov, J. K. Understanding Catalytic Activity Trends in the Oxygen Reduction Reaction. *Chem. Rev.* **2018**, *118* (5), 2302−2312.

(5) Man, I. C.; Su, H.-Y.; Calle-Vallejo, F.; Hansen, H. A.; Martínez, J. I.; Inoglu, N. G.; Kitchin, J.; Jaramillo, T. F.; Nørskov, J. K.; Rossmeisl, J. Universality in Oxygen Evolution Electrocatalysis on Oxide Surfaces. *ChemCatChem.* **2011**, *3* (7), 1159−1165.

(6) Siahrostami, S.; Tsai, C.; Karamad, M.; Koitz, R.; García-Melchor, M.; Bajdich, M.; Vojvodic, A.; Abild-Pedersen, F.; Nørskov, J. K.; Studt, F. Two-Dimensional Materials as Catalysts for Energy Conversion. *Catal. Lett.* **2016**, *146* (10), 1917−1921.

(7) Busch, M.; Halck, N. B.; Kramm, U. I.; Siahrostami, S.; Krtil, P.; Rossmeisl, J. Beyond the Top of the Volcano? − A Unified Approach to Electrocatalytic Oxygen Reduction and Oxygen Evolution. *Nano Energy* **2016**, *29*, 126.

(8) Siahrostami, S.; Björketun, M. E.; Strasser, P.; Greeley, J.; Rossmeisl, J. Tandem Cathode for Proton Exchange Membrane Fuel Cells. *Phys. Chem. Chem. Phys.* **2013**, *15* (23), 9326−9334.

(9) Koper, M. T. M. Theory of Multiple Proton−Electron Transfer Reactions and Its Implications for Electrocatalysis. *Chem. Sci.* **2013**, *4* (7), 2710.

(10) Vojvodic, A.; Nørskov, J. K. New Design Paradigm for Heterogeneous Catalysts. *Natl. Sci. Rev.* **2015**, *2* (2), 140−149.

(11) Sours, T.; Patel, A.; Nørskov, J.; Siahrostami, S.; Kulkarni, A. Circumventing Scaling Relations in Oxygen Electrochemistry Using Metal−Organic Frameworks. *J. Phys. Chem. Lett.* **2020**, *11* (23), 10029−10036.

(12) Wan, H.; Østergaard, T. M.; Arnarson, L.; Rossmeisl, J. Climbing the 3D Volcano for the Oxygen Reduction Reaction Using Porphyrin Motifs. *ACS Sustain. Chem. Eng.* **2019**, *7* (1), 611−617.

(13) Doyle, A. D.; Montoya, J. H.; Vojvodic, A. Improving Oxygen Electrochemistry through Nanoscopic Confinement. *ChemCatChem.* **2015**, *7* (5), 738−742.

(14) Busch, M.; Halck, N. B.; Kramm, U. I.; Siahrostami, S.; Krtil, P.; Rossmeisl, J. Beyond the Top of the Volcano? − A Unified Approach to Electrocatalytic Oxygen Reduction and Oxygen Evolution. *Nano Energy* **2016**, *29*, 126−135.

(15) Fukuzumi, S.; Yamada, Y.; Karlin, K. D. Hydrogen Peroxide as a Sustainable Energy Carrier: Electrocatalytic Production of Hydrogen Peroxide and the Fuel Cell. *Electrochim. Acta* **2012**, *82*, 493−511.

(16) McDonnell-Worth, C. J.; MacFarlane, D. R. Progress towards Direct Hydrogen Peroxide Fuel Cells (DHPFCs) as an Energy Storage Concept. *Aust. J. Chem.* **2018**, *71* (10), 781−788.

(17) Luo, N.; Miley, G. H.; Shrestha, P. J.; Gimlin, R.; Burton, R.; Rusek, J.; Holcomb, F. H2O2-Based Fuel Cells for Space Power Systems. *Collect. Technol. Pap. - 3rd Int. Energy Convers. Eng. Conf.* **2005**, *3*, 1947−1967.

(18) Marsh, C.; Licht, S. A Novel Aqueous Dual-Channel Aluminum-Hydrogen Peroxide Battery. *J. Electrochem. Soc.* **1994**, *141* (6), 61−63.

(19) Xu, L.; Liu, J.; Chen, P.; Wang, Z.; Tang, D.; Liu, X.; Meng, F.; Wei, X. High-Power Aqueous Zn-H2O2 Batteries for Multiple Applications. *Cell Reports Phys. Sci.* **2020**, *1* (3), 100027.

(20) Siahrostami, S.; Villegas, S. J.; Bagherzadeh Mostaghimi, A. H.; Back, S.; Farimani, A. B.; Wang, H.; Persson, K. A.; Montoya, J. A Review on Challenges and Successes in Atomic-Scale Design of Catalysts for Electrochemical Synthesis of Hydrogen Peroxide. *ACS Catal.* **2020**, *10* (14), 7495−7511.

(21) Yang, S.; Verdaguer-Casadevall, A.; Arnarson, L.; Silvioli, L.; Čolić, V.; Frydendal, R.; Rossmeisl, J.; Chorkendorff, I.; Stephens, I. E. L. Toward the Decentralized Electrochemical Production of H2O2: A Focus on the Catalysis. *ACS Catal.* **2018**, *8* (5), 4064−4081.

(22) Fuku, K.; Miyase, Y.; Miseki, Y.; Funaki, T.; Gunji, T.; Sayama, K. Photoelectrochemical Hydrogen Peroxide Production from Water on a WO3/BiVO4 Photoanode and from O2 on an Au Cathode without External Bias. *Chem. - An Asian J.* **2017**, *12*, 1111.

(23) Siahrostami, S.; Li, G.-L.; Viswanathan, V.; Nørskov, J. K. One- or Two-Electron Water Oxidation, Hydroxyl Radical, or H_2O_2 Evolution. *J. Phys. Chem. Lett.* **2017**, *8*, 1157−1160.

(24) Shi, X.; Siahrostami, S.; Li, G.-L.; Zhang, Y.; Chakthranont, P.; Studt, F.; Jaramillo, T. F.; Zheng, X.; Nørskov, J. K. Understanding Activity Trends in Electrochemical Water Oxidation to Form Hydrogen Peroxide. *Nat. Commun.* **2017**, *8* (1), 701.

(25) Xia, C.; Back, S.; Ringe, S.; Jiang, K.; Chen, F.; Sun, X.; Siahrostami, S.; Chan, K.; Wang, H. Confined Local Oxygen Gas Promotes Electrochemical Water Oxidation to Hydrogen Peroxide. *Nat. Catal.* **2020**, *3* (2), 125−134.

(26) Kelly, S. R.; Shi, X.; Back, S.; Vallez, L.; Park, S. Y.; Siahrostami, S.; Zheng, X.; Nørskov, J. K. ZnO As an Active and Selective Catalyst for Electrochemical Water Oxidation to Hydrogen Peroxide. *ACS Catal.* **2019**, *9* (5), 4593−4599.

(27) Park, S. Y.; Abroshan, H.; Shi, X.; Jung, H. S.; Siahrostami, S.; Zheng, X. CaSnO3: An Electrocatalyst for Two-Electron Water Oxidation Reaction to Form H2O2. *ACS Energy Lett.* **2019**, *4* (1), 352−357.

(28) Baek, J. H.; Gill, T. M.; Abroshan, H.; Park, S.; Shi, X.; Nørskov, J.; Jung, H. S.; Siahrostami, S.; Zheng, X. Selective and Efficient Gd-Doped BiVO4 Photoanode for Two-Electron Water Oxidation to H2O2. *ACS Energy Lett.* **2019**, *4*, 720−728.

(29) Izgorodin, A.; Izgorodina, E.; MacFarlane, D. R. Low Overpotential Water Oxidation to Hydrogen Peroxide on a MnOx Catalyst. *Energy Environ. Sci.* **2012**, *5* (11), 9496.

(30) Fuku, K.; Miyase, Y.; Miseki, Y.; Gunji, T.; Sayama, K. Enhanced Oxidative Hydrogen Peroxide Production on Conducting Glass Anodes Modified with Metal Oxides. *ChemistrySelect* **2016**, *1* (18), 5721−5726.

(31) Viswanathan, V.; Hansen, H. A.; Nørskov, J. K. Selective Electrochemical Generation of Hydrogen Peroxide from Water Oxidation. *J. Phys. Chem. Lett.* **2015**, *6* (21), 4224−4228.

(32) Koper, M. T. M. Thermodynamic Theory of Multi-Electron Transfer Reactions: Implications for Electrocatalysis. *J. Electroanal. Chem.* **2011**, *660* (2), 254−260.

(33) Shi, X.; Back, S.; Gill, T. M.; Siahrostami, S.; Zheng, X. Electrochemical Synthesis of H2O2 by Two-Electron Water Oxidation Reaction. *Chem.* **2021**, *7* (1), 38−63.
(34) Montoya, J. H.; Doyle, A. D.; Nørskov, J. K.; Vojvodic, A. Trends in Adsorption of Electrocatalytic Water Splitting Intermediates on Cubic ABO3 Oxides. *Phys. Chem. Chem. Phys.* **2018**, *20* (5), 3813−3818.
(35) Jain, A.; Ong, S. P.; Hautier, G.; Chen, W.; Richards, W. D.; Dacek, S.; Cholia, S.; Gunter, D.; Skinner, D.; Ceder, G.; et al. Commentary: The Materials Project: A Materials Genome Approach to Accelerating Materials Innovation. *APL Mater.* **2013**, *1* (1), 011002.
(36) Persson, K. A.; Waldwick, B.; Lazic, P.; Ceder, G. Prediction of Solid-Aqueous Equilibria: Scheme to Combine First-Principles Calculations of Solids with Experimental Aqueous States. *Phys. Rev. B* **2012**, *85* (23), 235438.
(37) Ong, S. P.; Richards, W. D.; Jain, A.; Hautier, G.; Kocher, M.; Cholia, S.; Gunter, D.; Chevrier, V. L.; Persson, K. A.; Ceder, G. Python Materials Genomics (Pymatgen): A Robust, Open-Source Python Library for Materials Analysis. *Comput. Mater. Sci.* **2013**, *68*, 314−319.
(38) Patel, A.; Nørskov, J. K.; Persson, K. A.; Montoya, J. H. Efficient Pourbaix Diagrams of Many-Element Compounds. *Phys. Chem. Chem. Phys.* **2019**, *21*, 1−11.
(39) Singh, A. K.; Zhou, L.; Shinde, A.; Suram, S. K.; Montoya, J. H.; Winston, D.; Gregoire, J. M.; Persson, K. A. Electrochemical Stability of Metastable Materials. *Chem. Mater.* **2017**, *29* (23), 10159−10167.
(40) Shi, X.; Siahrostami, S.; Li, G.-L.; Zhang, Y.; Chakthranont, P.; Studt, F.; Jaramillo, T. F.; Zheng, X.; Nørskov, J. K. Understanding Activity Trends in Electrochemical Water Oxidation to Form Hydrogen Peroxide. *Nat. Commun.* **2017**, *8* (1), 701.
(41) Shi, X.; Siahrostami, S.; Li, G.-L.; Zhang, Y.; Chakthranont, P.; Studt, F.; Jaramillo, T. F.; Zheng, X.; Nørskov, J. K. Understanding Activity Trends in Electrochemical Water Oxidation to Form Hydrogen. *Nat. Commun.* **2017**, No. SEPT, 1−12.
(42) Gao, W.; Zhang, W.; Tian, B.; Zhen, W.; Wu, Y.; Zhang, X.; Lu, G. Visible Light Driven Water Splitting over CaTiO3/Pr3+-Y2SiO5/RGO Catalyst in Reactor Equipped Artificial Gill. *Appl. Catal. B Environ.* **2018**, *224*, 553−562.
(43) Patial, S.; Hasija, V.; Raizada, P.; Singh, P.; Khan Singh, A. A. P.; Asiri, A. M. Tunable Photocatalytic Activity of SrTiO3 for Water Splitting: Strategies and Future Scenario. *J. Environ. Chem. Eng.* **2020**, *8* (3), 103791.
(44) Kumar, M.; Srikanth, S.; Ravikumar, B.; Alex, T. C.; Das, S. K. Synthesis of Pure and Sr-Doped LaGaO3, LaFeO3 and LaCoO3 and Sr,Mg-Doped LaGaO3 for ITSOFC Application Using Different Wet Chemical Routes. *Mater. Chem. Phys.* **2009**, *113* (2), 803−815.
(45) Hasegawa, S.; Shimotani, K.; Kishi, K.; Watanabe, H. Electricity Generation from Decomposition of Hydrogen Peroxide. *Electrochem. Solid-State Lett.* **2005**, *8* (2), 119−122.
(46) Cao, D.; Sun, L.; Wang, G.; Lv, Y.; Zhang, M. Kinetics of Hydrogen Peroxide Electroreduction on Pd Nanoparticles in Acidic Medium. *J. Electroanal. Chem.* **2008**, *621* (1), 31−37.
(47) Kjeang, E.; Brolo, A. G.; Harrington, D. A.; Djilali, N.; Sinton, D. Hydrogen Peroxide as an Oxidant for Microfluidic Fuel Cells. *J. Electrochem. Soc.* **2007**, *154* (12), B1220.
(48) Cao, D.; Chao, J.; Sun, L.; Wang, G. Catalytic Behavior of Co3O4 in Electroreduction of H2O2. *J. Power Sources* **2008**, *179* (1), 87−91.
(49) Nath, N. C. D.; Debnath, T.; Kim, E.-K.; Ali Shaikh, M. A.; Lee, J.-J. Nanostructured Copper−Cobalt Based Spinel for the Electrocatalytic H2O2 Reduction Reaction. *Electrochim. Acta* **2018**, *273*, 474−482.
(50) Poux, T.; Bonnefont, A.; Ryabova, A.; Kéranguéven, G.; Tsirlina, G. A.; Savinova, E. R. Electrocatalysis of Hydrogen Peroxide Reactions on Perovskite Oxides: Experiment versus Kinetic Modeling. *Phys. Chem. Chem. Phys.* **2014**, *16* (27), 13595−13600.
(51) Cardoso, D. S. P.; Šljukić, B.; Sousa, N.; Sequeira, C. A. C.; Figueiredo, F. M. L.; Santos, D. M. F. On the Stability in Alkaline Conditions and Electrochemical Performance of A2BO4-Type Cathodes for Liquid Fuel Cells. *Phys. Chem. Chem. Phys.* **2018**, *20* (28), 19045−19056.
(52) Yunphuttha, C.; Porntheeraphat, S.; Wongchaisuwat, A.; Tangbunsuk, S.; Marr, D. W. M.; Viravathana, P. Characterization of La1-: XSrxMnO3 Perovskite Catalysts for Hydrogen Peroxide Reduction. *Phys. Chem. Chem. Phys.* **2016**, *18* (25), 16786−16793.
(53) Man, I. C.; Su, H.-Y.; Calle-Vallejo, F.; Hansen, H. A.; Martínez, J. I.; Inoglu, N. G.; Kitchin, J.; Jaramillo, T. F.; Nørskov, J. K.; Rossmeisl, J. Universality in Oxygen Evolution Electrocatalysis on Oxide Surfaces. *ChemCatChem.* **2011**, *3* (7), 1159−1165.

https://doi.org/10.1021/acsenergylett.2c01417
ACS Energy Lett. 2022, 7, 2717−2724